February 2001 • NREL/SR-520-29504

Subcontractor Report

Electroabsorption and Transport Measurements and Modeling Research in Amorphous Silicon Based Solar Cells

Annual Report
24 March 1999–23 March 2000

E. A. Schiff, N. Kopidakis, J. Lyou, S. Rane, Q. Yuan, and K. Zhu
Syracuse University
Syracuse, New York

National Renewable Energy Laboratory

1617 Cole Boulevard
Golden, Colorado 80401-3393

NREL is a U.S. Department of Energy Laboratory
Operated by Midwest Research Institute • Battelle • Bechtel

Contract No. DE-AC36-99-GO10337

February 2001 • NREL/SR-520-29504

Electroabsorption and Transport Measurements and Modeling Research in Amorphous Silicon Based Solar Cells

Annual Report
24 March 1999–23 March 2000

E. A. Schiff, N. Kopidakis, J. Lyou, S. Rane, Q. Yuan, and K. Zhu
Syracuse University
Syracuse, New York

NREL Technical Monitor: Bolko von Roedern

Prepared under Subcontract No. XAK-8-17619-23

National Renewable Energy Laboratory

1617 Cole Boulevard
Golden, Colorado 80401-3393

NREL is a U.S. Department of Energy Laboratory
Operated by Midwest Research Institute • Battelle • Bechtel

Contract No. DE-AC36-99-GO10337

Available electronically at http://www.doe.gov/bridge

Available for a processing fee to U.S. Department of Energy
and its contractors, in paper, from:
U.S. Department of Energy
Office of Scientific and Technical Information
P.O. Box 62
Oak Ridge, TN 37831-0062
phone: 865.576.8401
fax: 865.576.5728
email: reports@adonis.osti.gov

Available for sale to the public, in paper, from:
U.S. Department of Commerce
National Technical Information Service
5285 Port Royal Road
Springfield, VA 22161
phone: 800.553.6847
fax: 703.605.6900
email: orders@ntis.fedworld.gov
online ordering: http://www.ntis.gov/ordering.htm

Printed on paper containing at least 50% wastepaper, including 20% postconsumer waste

Preface

This research project has two broad objectives:

- We seek a deeper understanding of the open circuit voltage V_{OC} in amorphous silicon based solar cells, and in particular we wish to determine whether the present open-circuit voltages in these cells can be increased. We combine experimental studies of device operation with solar cell modeling.
- We seek to measure and to understand electron and hole photocarrier drift under electric fields for the technologically significant forms of amorphous-silicon based materials. We incorporate this knowledge into solar cell device models in an effort to deepen our understanding of solar cell operation.

In addition to the support from the National Renewable Energy Laboratory, this research received support from the Korea Research Foundation and from Korea University for Prof. Lyou's research leave at Syracuse University.

Summary

In Phase II of this project we have done significant work on the following topics:

1. *Solar cell modeling employing the AMPS computer program.* We have drawn a preliminary conclusion that present open-circuit voltages in amorphous silicon based cells are limited by interface properties, despite certain evidence that the absorber layer is the limiting factor. We have studied interface limitation using the AMPS computer simulation code, and proposed a "thermionic emission" model for open-circuit voltage limitation by the *p/i* interface. Most of the contents of this report are included in a forthcoming paper: L. Jiang, J. H. Lyou, S. Rane, E. A. Schiff, Q. Wang, and Q. Yuan, *Materials Research Society Symposium Proceedings Vol. 609*, in press.
2. *Drift-mobility measurements in a-Si:H made with high hydrogen dilution.* We have continued work on new amorphous-silicon based materials with improved hole hole drift mobilities. The work this phase continued drift-mobility measurements in several *n/i/m* cells from Pennsylvania State University with a-Si absorber layers made under maximal hydrogen dilution. We find a modest *increase* in hole mobility in these materials compared to conventional a-Si:H; the measurements are in satisfactory agreement with the standard valence bandtail multiple-trapping model with a bandtail width parameter of about 40 meV.
3. *Electroabsorption spectroscopy in solar cells.* An unexpected byproduct of our work estimating V_{bi} has been discovery and interpretation of an infrared absorption band near 1.0 eV. We believe that this band is due to dopants & defects at the *n/i* interface of the cells; we are particularly excited by this result because it involves a new type of interface-spectroscopy for working solar cells. In the present report we discuss the possibility that the spectrum is evidence for defect complexing. Collaborators in this work include Steven Hegedus (Institute of Energy Conversion, Univ. of Delaware), Gautam Ganguly (Solarex Thin Films Division), Jeff Yang and Subhendu Guha (United Solar Systems Corp.), and Richard Crandall (National Renewable Energy Laboratory). Most of the contents of this report have been published: J. H. Lyou, N. Kopidakis, and E. A. Schiff, *J. Non-Cryst. Solids* **266-269**, 227-231 (2000)
4. *Hydrogen-mediated models for defect metastability in amorphous silicon.* We have made a particular proposal for how to marry the "hydrogen-collision" model for illumination-induced metastabilities in the defect density of a-Si:H with the "clustered hydrogen" model for thermally-generated metastabilities. Hydrogen-mediated models must account for both types of metastability. Most of the contents of this section have been published: N. Kopidakis and E. A. Schiff, *J. Non-Cryst. Solids* **266-269**, 415-418 (2000).

Table of Contents

Table of Figures

Computer Modeling Studies

Abstract

We have performed computer calculations to explore effects of the *p/i* interface on the open-circuit voltage in a-Si:H based *pin* solar cells. The principal conclusions are that interface limitation can occur for values of V_{OC} significantly below the built-in potential V_{BI} of a cell, and that the effects can be understood in terms of thermionic emission of electrons from the intrinsic layer into the *p*-layer. We compare measurements of V_{OC} and electroabsorption estimates of V_{BI} with the model calculations. We conclude that *p/i* interface limitation is important for current a-Si:H based cells, and that the conduction band offset between the *p* and *i* layers is as important as the built-in potential for future improvements to V_{OC}.

Introduction

The open-circuit voltage V_{oc} of amorphous silicon (a-Si:H) based *pin* solar cells remains the most ill-understood of its device parameters. This lack of insight is remarkable, since the experimental behavior of V_{OC} is generally quite simple. V_{OC} depends little upon the defect density or thickness of the intrinsic layer, and eV_{OC} is roughly shifted down from the optical bandgap of this layer by about 0.8-0.9 eV. Furthermore, the value of V_{OC} is mostly controlled by the fairly simple physics of the splitting of quasi-Fermi-levels in the intrinsic layer. Nonetheless, even the simplest question about it, which is whether V_{oc} is reduced by non-ideal *p/i* or *n/i* interfaces, is not conclusively answered. Of course, this unsatisfactory state of affairs does leave open the tantalizing possibility of significant improvements in V_{OC} – if only device-makers could be pointed in a better direction.

In this paper, we first review the interrelation of the open-circuit voltage and quasi-Fermi levels in the device physics of a-Si:H based *pin* solar cells. In cells with ideal *p* and *n* layers, V_{OC} reaches its "intrinsic limit," which may be equated to the splitting of the electron and hole quasi-Fermi levels in bulk intrinsic material. In principle V_{OC} measurements can become a very interesting alternative to photoconductivity measurements in intrinsic films. We next discuss the hypothesis that V_{OC} achieves this intrinsic limit for optimized a-Si:H cells, and we conclude that this hypothesis is most likely incorrect. First, open-circuit voltages do not exhibit the dependence upon defect density which is known to apply to quasi-Fermi levels for thin films of intrinsic a-Si:H. Second, we present electroabsorption measurements of the built-in potential in a-Si:H based solar cells which yield rather small values for V_{bi} (in the range 1.05 – 1.25 V). The built-in potential is generally recognized as the ultimate limit to V_{OC} in any solar cell. We present computer calculations which strongly suggest that the measured values are small enough to be reducing V_{OC} for the a-Si:H cells.

One unexpected result from the modeling work is that interface limitation can be significant even when V_{OC} is "significantly" (0.5 V) below the built-in potential. We present a computer simulation study of the mechanism by which non-ideal doped layers suppress V_{OC}, and we propose a "thermionic emission of minority carriers" model to explain the effect. The model shows that the conduction band offset between the *p* and *i* layers is as significant in determining V_{OC} and other cell properties as is the built-in potential V_{BI}.

V_{oc} and quasi-Fermi levels

In Figure 1 we illustrate profiles for several important levels in an amorphous-silicon based *pin* solar cell under open-circuit conditions. The profiles are calculated using a computer program (AMPS PC-1D [1]) and parameters we describe in more detail subsequently. The upper panel is calculated under thermal equilibrium conditions (the dark), and shows the conduction and valence bandedges E_C and E_V,

respectively, as well as the Fermi level E_F. The lower panel is calculated under illuminated conditions, and shows E_C, E_V, and the electron and hole quasi-Fermi levels E_{Fe} and E_{Fh}, respectively. By way of introduction, we now explain the equation between the measured open-circuit voltage under illumination and the separation of quasi-Fermi-levels. This well-known "theorem" proves to be a powerful tool in understanding open-circuit voltages in many solar cells, which can be very well illustrated using computer calculations.

We briefly review the definitions of these levels. For an amorphous semiconductor, E_C is usually identified with a mobility-edge dividing extended electron states (at higher level energies) from localized *bandtail* states (at lower level energies). Electrons occupying extended states are assumed to be mobile, and are characterized by an electron "band mobility" μ_e. Electrons occupying the localized states are immobile (or *trapped*). This relatively simple model, in conjunction with the assumption that the bandtail states have an exponential distribution, accounts well for direct drift-mobility measurements for both electrons and holes. The electron quasi-Fermi level E_{Fe} is actually just a bookkeeping device for keeping track of the density of mobile electrons n under illumination [2,3]. Under thermal equilibrium (dark) conditions, we would calculate n from the expression $n = N_C \exp(-(E_C - E_F)/kT)$, where N_C is an "effective density-of-states" for the extended, conduction band states and E_F is the Fermi-energy. Under illumination, we define E_{Fe} implicitly from the definition: $n_{photo} = N_C \exp(-(E_C - E_{Fe})/kT)$. Similar definitions apply to holes and the valence band.

Returning to Figure 1, in the upper panel note the constancy of E_F (indicating that the different layers are in thermal equilibrium), and also note the decline in E_C across the cell. Spatial variation in E_C indicates that there is a "built-in" electric field driving electrons from left to right. The built-in field arises because electrons have been transferred from the n layer to the p layer in order to establish thermal equilibrium between the n and p layers, which have different Fermi energies relative to vacuum. The built-in potential V_{BI} is about 1.6 V for this calculation.

Under illumination, strongly non-equilibrium conditions are created. The middle portion of the cell becomes nearly free of electric field, and may be viewed as a slice of "bulk" intrinsic material. The zero of the vertical scale was set by the electron quasi-Fermi level E_F in the n-layer. E_{Fe} is essentially constant in the n-type and intrinsic layers. In the p-layer, there is a return to thermal-equilibrium conditions as indicated by the convergence of E_{Fe} and E_{Fh}. This effect arises from the much larger recombination rate of electrons in the p-layer

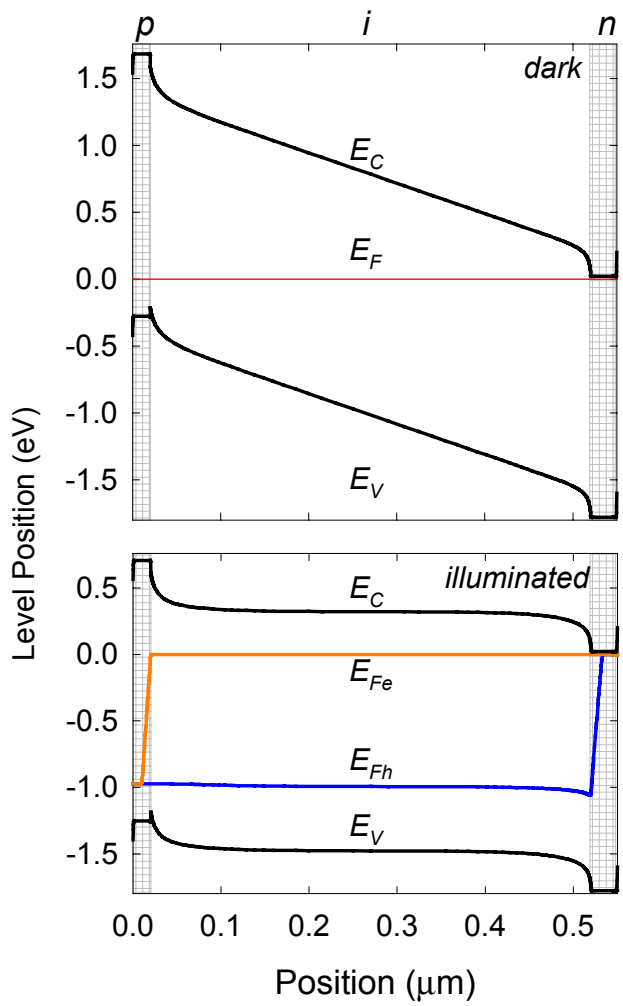

Fig. 1: Computer calculation of open-circuit profiles in an a-Si:H based *pin* solar cell for the conduction and valence bandedges (E_C and E_V) and of the Fermi level E_F (dark) or of the electron and hole quasi-Fermi levels (E_{Fe} and E_{Fh} - illuminated). The open-circuit voltage is precisely the value of E_{Fh} at the left interface ($x = 0$).

vis a vis the intrinsic layer; there are far more holes trapped near E_{Fh} in the p-layer than in the intrinsic layer. A corresponding argument applies in the *n*-layer.

The *open-circuit voltage* V_{OC} is measured across the terminals of the cell; the computer calculation yields 0.99 V. V_{OC} may be equated to the difference in Fermi levels between the left and right termals of the cell:

$$eV_{OC} = \left(E_F(x_L) - E_F(x_R)\right) \ . \tag{1}$$

As can be seen from the figure, eV_{OC} is simply the difference between $E_{Fh}(0)$ and $E_{Fe}(0.55)$.

Is V_{OC} determined solely by intrinsic-layer properties?

For the parameter set used for Figure 1, interface effects are unimportant: quasi-Fermi levels are essentially constant throughout the cell, and there is a "field-free" zone in the middle of the cell. We conclude that, for these conditions, V_{OC} may be equated to the separation between the electron and hole quasi-Fermi levels E_{fe} and E_{Fh} for intrinsic films of a-Si:H:

$$eV_{OC} = \left(E_{Fe} - E_{Fh}\right) \ , \tag{2}$$

where *e* is the electronic charge [4]. We now attempt to establish whether this simplest case, that open-circuit voltages are determined simply by the photoconductivity of the intrinsic-layer material, applies in optimized a-Si:H solar cells.

V_{OC} isn't correlated with defect densities

It appears well accepted by device-makers that there is little correlation between V_{oc} and the density of deep levels N_D (usually presumed to be dangling bonds) in a-Si:H. One paper shows that the defect density in intrinsic films could be increased nearly thirtyfold by light-soaking, while V_{OC} diminished by about 0.03 V [5].

The expected decrease in V_{OC} as the defect density changes may be calculated from the changes in the quasi-Fermi-levels for electrons and holes. The corresponding decline in the photoconductivity of a-Si:H films is roughly proportional to the reciprocal density [6]. Since the photoconductivity is electron-dominated, one may estimate the decline in the electron quasi-Fermi level ΔE_{Fe} simply:

$$\Delta E_{Fe} / kT = \ln\left(N_D^f / N_D^i \right) \ . \tag{3}$$

One obtains an expected decline of V_{OC} of about 0.09 eV due to this effect, which is substantially larger than the observed decline. A smaller effect, which further reduces V_{OC} is due to changes in the hole quasi-Fermi-level E_{Fh} as the defect density rises.

It is clear that the myriad of photoconductivity measurements on a-Si:H have at best an uncertain relationship to V_{OC}. The alternative is that V_{OC} is determined by photoconductivity effects in the interface regions. Indeed the present argument favoring interface effects would be conclusive if defect density changes as large as those in films were observed in *pin* cells, but effects this large have not (to our knowledge) been reported.

Crossover from intrinsic to interface limitation of V_{OC} is not abrupt

The simplest perspective on interface limitation of V_{OC} is the following. It is reasonable that V_{OC} cannot exceed V_{BI}; inspection of Figure 1 shows that V_{OC} is reduced from V_{BI} by electrostatic barriers at each

interface. One might therefore guess that, for low photogeneration rates G, V_{OC} should be dominated by intrinsic-layer quasi-Fermi-levels; for higher photogeneration rates there will be a crossover to the value $V_{OC} \approx V_{BI}$.

This perspective is profoundly misleading, as we now illustrate. Crossover from intrinsic-layer to interface limitation of V_{OC} occurs over many orders of magnitude of G, and can set in when V_{OC} is much below V_{BI}.

In Figure 2 we present calculations of V_{oc} for varying (uniform) photogeneration rates. We chose band and bandtail parameters based on a variety of fundamental measurements; the details are presented in the Appendix. For these calculations, intrinsic layer defects were not incorporated, since V_{OC} is not much affected by them. The uppermost, solid bold line is the result of an analytical calculation developed by Tiedje some years ago [7] which exploits the equation of V_{OC} with quasi-Fermi level splitting in the intrinsic layer. This calculation establishes what may be termed the *intrinsic limit* $V_{OC}^{intrinsic}$, by which we mean the upper limit determined only by the photoconductivity of the intrinsic layer itself.

For the AMPS calculations, the *n*-layer Fermi energy was set 0.1 eV below the conduction band, and had the same bandedges as the intrinsic-layer. We expect these parameters to adequately model a-Si:H:P *n*-layers. The *p*-layer bandgap was set to 1.96 eV, with symmetrical 0.08 eV offsets between the p-layer and intrinsic-layer bandedges. These parameters nominally describe a-SiC *p*-layers. The *p*-layer Fermi energy was adjusted to yield the several values of the built-in potential shown in the figure. The points calculated for V_{bi} =1.52 V approach the results of the analytical calculation for V_{OC} based on intrinsic layer properties alone. The consistency between the analytical and computer calculation is noteworthy.

Built-in potentials are small enough to affect V_{OC}

The points for V_{bi} = 1.32 V fall away significantly from the intrinsic-layer limit due to interface limitation by the *p/i* interface. We note two aspects of this behavior. First, interface limitation is important even when V_{OC} is substantially (0.4 V) less than V_{bi}. Second, the power-law, functional form of the dependence of V_{oc} upon G gives little indication that V_{OC} has been reduced by the interface. The crossover from intrinsic limitation (at low G) to interface limitation (at high G, as V_{OC} begins to approach V_{BI}): the interface causes an extremely soft effect on V_{OC} , which is stretched over many decades of generation rate.

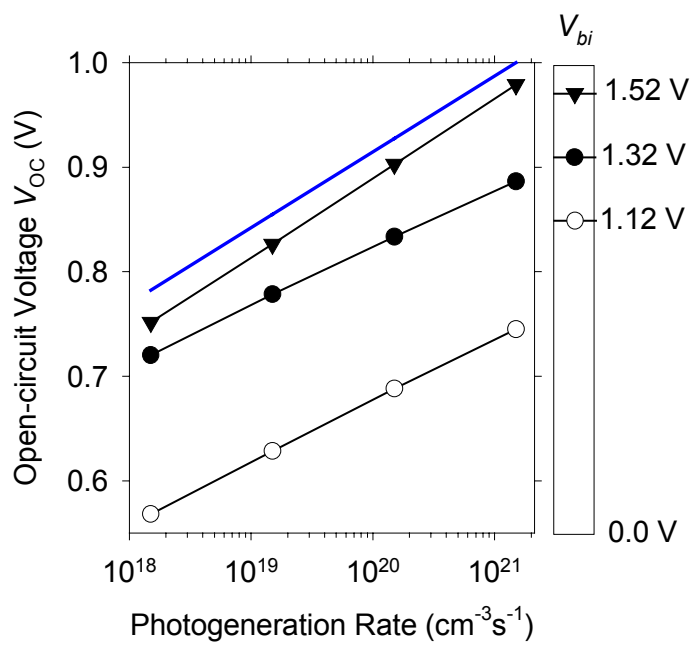

Fig. 2: Calculations of the dependence of the open-circuit voltage upon photogeneration rate for *pin* solar cells. The bold solid line is an analytical calculation based on intrinsic layer properties alone. The symbols plotted for different V_{bi} are based on computer calculations for varying Fermi-energies in the *p*-layer.

Does the p-layer reduce V_{OC} in optimized a-Si:H devices? To our knowledge, the best elaborated experimental estimates of V_{bi} in a-Si:H based *pin* solar cells are based on the small, electroabsorption effect [8]. In practice, one measures the modulated transmittance S due to sinusoidal

modulation δE of the electric field across the cell. This signal depends linearly upon the constant, DC voltage V across the cell:

$$S \propto \delta E(V - V_0).$$

Note that there is an offset voltage V_0. Under ideal conditions, V_0 determines the "built-in" potential.

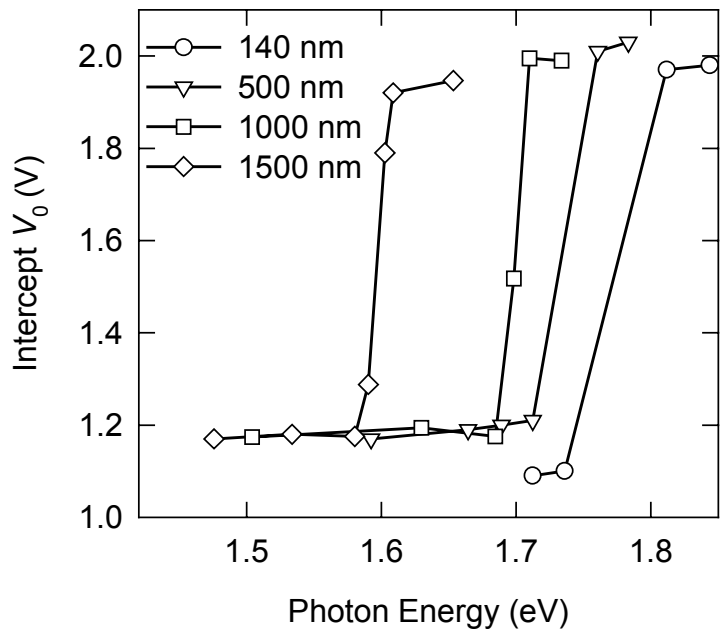

Fig. 3: Wavelength dependence of the electromodulated reflectance offset potential V_0 for four *nip* solar cells with a-SiGe:H absorber layers of differing thicknesses. The typical optical gap was 1.5 eV. The long-wavelength limit of about 1.15 V is an estimate of the built-in potential.

In Figure 3 we present a summary of the results for V_0 as a function of the wavelength for a series of *pin* cells incorporating a-SiGe intrinsic layers with varying intrinsic-layer thicknesses and bandgaps; the cells were prepared at United Solar Systems Corp. The doped layers were deposited under the same conditions for all of these cells. The *n*-layer was a-Si:H:P; the *p*-layer was microcrystalline Si:B [9].

A full interpretation of these measurements is more complicated than the simplified description above implies, and will not be given here. For these cells the optical measurements were actually reflectance, not transmittance. For smaller optical energies incident illumination travels through the cell and is reflected at the back surface; the measured reflection modulation is dominated by the back-surface reflected beam. As can be seen in the figure, several cells yield $V_0 \approx 1.15$ V in this regime. For shorter wavelengths the incident beam is too strongly absorbed to reach the back surface, and the measured signal is essentially true electroreflectance. We have not yet found a convincing explanation for the value $V_0 \approx 2.0$. From these data and our prior work, we conclude that $1.05 < V_{BI} < 1.25$ for the range of cells we have studied, including our work with both microcrystalline Si and amorphous SiC p-layers.

In conjunction with the simulation results in Figure 2, this range of values for V_{BI} is plainly small enough to suggest that V_{OC} is probably reduced by the *p/i* interface in working cells. In the next section we present a discussion of the device physics which underlies this effect.

Device Physics of the *P/I* Interface

In Figure 4 we present open-circuit profiles for an AMPS calculation with the parameters of Fig. 2 ($V_{bi} = 1.32$ V, $G = 1.5\times10^{21}$ cm^{-3}). As can be inferred from the bottom right panel of the figure, the diminishment is associated entirely with the gradient $e\Delta V^{p/i}$ in E_{Fh} as it crosses through the *p/i* interface: the separation between E_{Fe} and E_{Fh} in the central, field-free zone remains at its intrinsic limit of about 1.0 V.

Non-constant profiles for E_{Fh} imply the existence of a corresponding hole current, in this case flowing from the intrinsic layer into the *p*-layer. We show the corresponding electron and hole current profiles in the figure also; since there is no net electrical current flowing under open-circuit conditions, the electron and hole currents cancel exactly. The fact that the electron current flows without an appreciable gradient

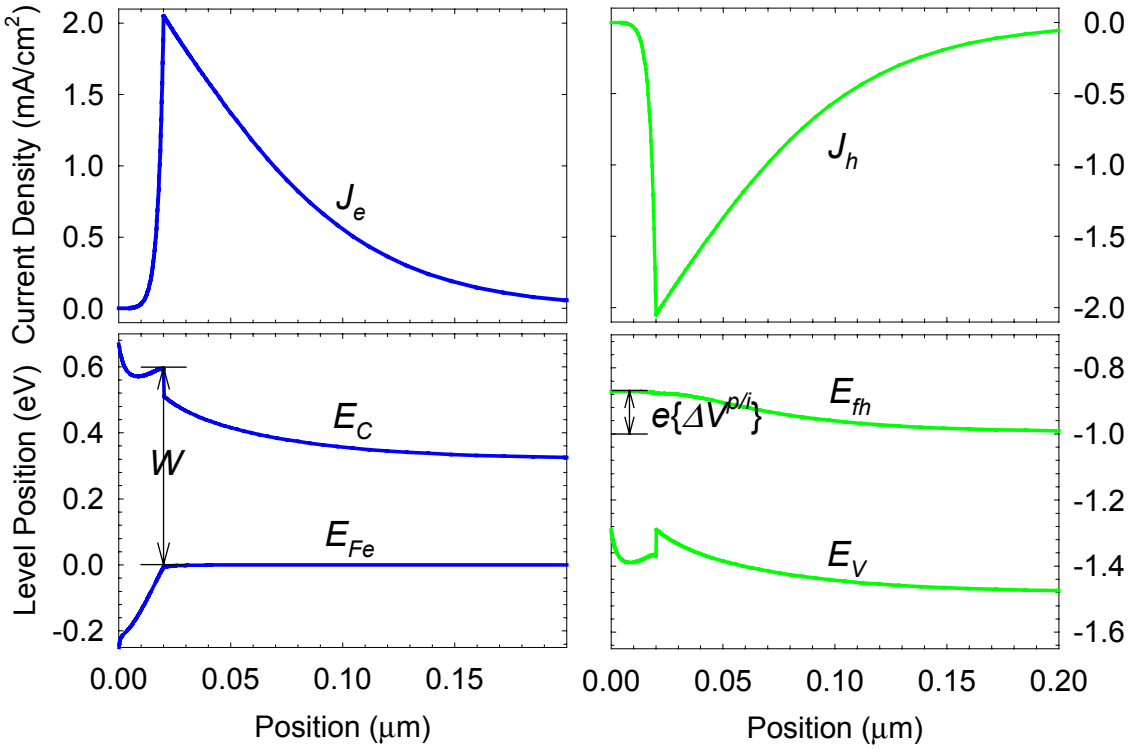

Fig. 4: Profiles calculated using AMPS and the common parameters described in the text. The built-in potential was set to 1.3 V by adjusting the doping level of the *p*-layer. Note the electron current J_e, which is a consequence of thermionic emission over the barrier W. While J_e flows without an appreciable gradient in E_{Fe}, the hole countercurrent J_h does require a noticeable gradient $e\Delta V^{p/i}$.

in E_{Fe} reflects the facts that E_{Fe} is closer to its band than E_{Fh}, as well as the larger band mobility chosen for electrons.

These currents reflect the transport of electrons and holes, which are photogenerated in the intrinsic layer into the *p*-layer, where they recombine quite close to the interface. Indeed the recombination current at the interface is readily computed from the sharp drop in J_e and J_h.at the interface. We were initially surprised by the existence of the electron current. As illustrated in the figure, there is a sizable electrostatic barrier W which impedes electron current into the *p*-layer.

These currents may be understood in terms of thermionic emission of electrons over the barrier W. In Figure 5 we show the logarithm of the recombination current as a function of the barrier height W. Currents associated with a given symbol were calculated by varying W using only the conduction band offset at the *p/i* interface $\Delta E_C^{p/i}$; all other parameters were unchanged. Different symbols correspond to different photogeneration rates; these change W by changing the electron quasi-Fermi level E_{Fe} in the intrinsic layer.

For a specific illumination, J_R is activated for larger barrier heights; the decline illustrated in the figure is consistent with $J_R \propto \exp(-W/kT))$. For smaller barrier heights, J_R is limited by the total photogeneration within a certain range from the *p/i* interface; we speculate that this range is the ambipolar diffusion length.

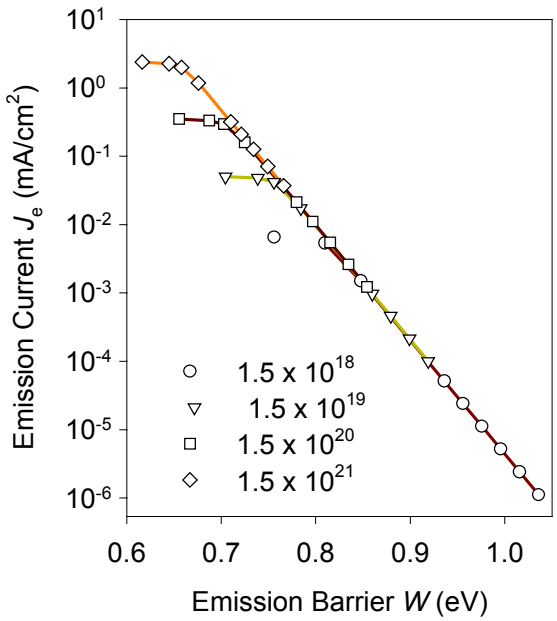

Fig. 5: Dependence of the electron current J_e at the *p/i* interface upon the barrier height W (see figure 4) for several different uniform generation rates. For each intensity, W was varied by changing only the conduction band offset at the *p/i* interface; $V_{BI} = 1.2$ V.

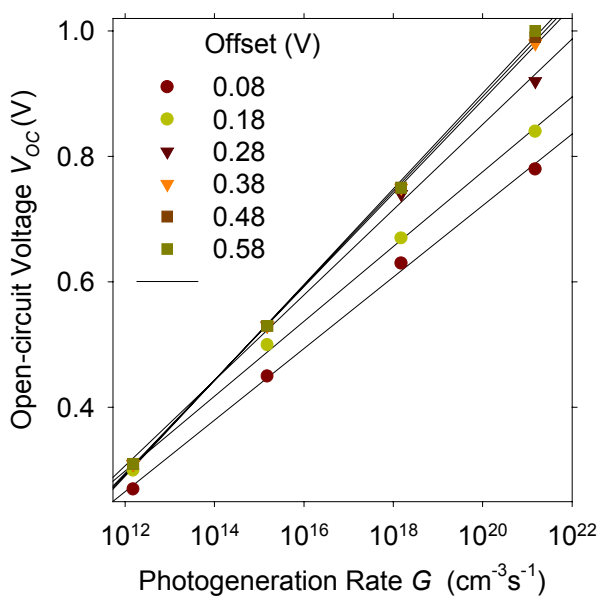

Fig. 6: Open-circuit voltage V_{OC} as a function of (uniform) photogeneration rate G; results for varying conduction band offset $\Delta E_C^{p/i}$ are given. Note that the built-in potential $V_{BI} = 1.2$ V does *not* change for these calculations.

In Figure 6 we present the dependence of V_{OC} upon photogeneration rate G for the same calculations used for Figure 5. We varied the band offsets $\Delta E_C^{p/i}$, and left the built-in potential constant at 1.2 V. Note the very large range of generation rates involved. For the larger values of $\Delta E_C^{p/i}$, V_{OC} lies on the *intrinsic limit* line throughout the range of G. However, as $\Delta E_C^{p/i}$ declines, V_{OC} breaks away progressively; V_{OC} is significantly diminished from the intrinsic limit $V_{OC}^{intrinsic}$ throughout the normal range of photogeneration rates, and adopts essentially the same power-law form as for the intrinsic limit.

Discussion

We have presented two results which militate against the simple model that open-circuit voltages achieve their intrinsic limit $V_{OC}^{intrinsic}$ in a-Si:H based *pin* solar cells. First, the unexpected robustness of V_{OC} as defect densities in the intrinsic layer are increased seems inexplicable in this model. Second, experimental estimates for V_{bi} are sufficiently small that, in conjunction with computer modeling of a-Si:H based cells, they argue for interface limitation of V_{OC}. To these results may be added other experiments which show that modification of the p/i interface region by inclusion of "buffer layers" of various types increases V_{OC} [10].

What is plainly required to advance open-circuit voltage physics is a satisfactory model for V_{OC} based on interface physics. We have developed a fairly satisfactory account for the computer calculations of *p/i* interface effects in terms of electron thermionic emission from the intrinsic layer into the *p*-layer which we believe can form the basis of an improved model. Nonetheless, we cannot claim at present to have a satisfactory understanding of V_{OC}. For example, the measured slopes of the logarithmic, V_{OC} vs. photogeneration rate in cells are steeper than the results of the computer calculation. We are, reluctantly, considering the possibility of more complex models for the *p/i* interface than the simple "heterostructure" model treated here. As one example, Branz and Crandall [11] have discussed thermodynamic defect generation at the *n/i* and *p/i* interfaces.

Appendix: bandtail parameters for solar cell modeling

This page contains a set of parameters based on a particular reading of the literature of direct experiments on photocarrier and optical processes in intrinsic amorphous silicon. In some cases modeling of solar cells may end up giving more reliable estimates. The parameter symbols are those used for the AMPS simulation program.

Parameter	*AMPS Symbol*	*Value*	*Notes and References*
Overall Electronic Properties			
Electrical Bandgap E_G	EG	1.80 eV	This parameter is surprisingly difficult to establish accurately; the best estimates appear to be those based on internal photoemission: Chen and Wronski [12].
Conduction Band Parameters			
Effective density of states N_C	NC	2.5×10^{20} cm^{-3}	Jackson, *et al.*[13] did a careful study of photoemission and related measurements, and suggested that *g(E)* near E_C (the conduction band mobility edge) is about 10^{22} cm^{-3}. N_C is roughly the product of *kT* and this value for *g(E)* near room-temperature.
Electron band mobility μ_e	MUN	2 cm^2/Vs	Schiff, *et al.*[14] found that this value applies from essentially the moment of photogeneration throughout the picosecond domain. Larger values can be excluded both from this work and work by Juska, *et al.* [15].
Bandtail width	EA0	0.022	Wang, *et al.*[16].
Bandtail prefactor	GA0	10^{22} cm^{-3}eV^{-1}	See notes on NC. Note that NC = (kT)*GA0.
Bandtail cross-section ($B^0 + e^- -- B^-$)	TSIG/NA	2×10^{-16} cm^2	Wang, *et al.*[16] estimated $\nu = 5 \times 10^{11}$ s^{-1} for the "attempt-to-escape" frequency governing electron emission from the bandtail. "Detailed balance" $\nu = N_C b_T$ then constrains TSIG/NA, since b_T = (TSIG/NA)v_{thermal}.
Bandtail cross-section ($B^- + h^+ - B^0$)	TSIG/PA	10^{-16} cm^2	It is possible that this parameter has little effect on solar cell models. Nonetheless, we are not aware of any satisfactory experimental estimate of it. One might apply the "Langevin" expression for diffusion-limited capture of a free hole by a negatively-charged center, yielding perhaps 2×10^{-14} cm^2 [17]. This procedure doesn't work for electron capture by trapped holes, however.

Parameter	*AMPS Symbol*	*Value*	*Notes and References*
Valence Band Parameters			
Effective density of states	NV	2.5×10^{20} cm^{-3}	cf. Jackson, *et al.*[13]; see note for NC.
Hole band mobility	MUP	0.27 cm^2/Vs	Gu, *et al.* [18] have collected hole drift-mobility measurements and suggested this fitting for "standard" a-Si:H.
Bandtail width	ED0	0.048 eV	Basically set using Urbach tail. This value is conventional; see Gu, *et al.* [18] for estimates based on hole drift mobilities.
Bandtail prefactor	GD0	10^{22} cm^{-3} eV^{-1}	Jackson, *et al.* [13]. See note for NV.
Bandtail cross-section ($B^0 + h^+ -- B^+$)	TSIG/PD	3×10^{-17} cm^2	Based on NU = 7.7×10^{10} s^{-1} from Gu, *et al.* [18]. See note for TSIG/NA
Bandtail cross-section ($B^+ + e^- -- B^0$)	TSIG/ND	10^{-16} cm^2	Juska, *et al.* [19] have inferred this parameter from subnanosecond recombination experiments. A slightly larger value was reported by Stradins, *et al.* [20]. These values are much smaller than expected from a fundamental argument due to Langevin; no one seems to understand the reason for such small values (see Schiff, 1995).

A note about capture cross-sections

It is conventional, and regrettable, that capture rates of photocarriers into localized states are described using cross sections. Rates for capture of a photocarrier are usually written in the form $R = bN$,where N is the density of some type of level which captures photocarriers, R is the capture rate (in s^{-1}), and b is the "capture coefficient" (in cm^3s^{-1}). It is conventional to express b in terms of a cross section $b = \sigma * v_{th}$, where σ is the capture cross-section (in cm^2) and v_{th} is a "thermal velocity." This last expression is a legacy from atomic scattering, and is probably meaningless in amorphous silicon. By convention we simply take $v_{th} = 10^7$ cm/s and don't think about this further.

Hole Drift Mobilities in a-Si:H: Maximal Hydrogen Dilution and Related Samples

Abstract

In this Phase of our research contract we have continued our research on drift-mobilities in amorphous silicon materials with improved hole drift mobilities. In particular we have exended the research in the previous Phase by additional measurements on samples from Penn State University made using high hydrogen dilution of silane gas during deposition, and we have made a fairly thorough fitting study of the parameters for the standard, exponential bandtail trapping model. Hole drift-mobilities are about six times higher than for "standard" amorphous silicon. The valence bandtail width parameters in hydrogen-diluted materials are as small as 40 meV; this figure should be compared to the typical value of 48 meV in standard amophous hydrogenated silicon.

Introduction

Thin-film silicons made using silane gas diluted with hydrogen have structures ranging from amorphous to microcrystalline; a transition occurs as the hydrogen dilution is increased [21]. Amorphous silicon layers made at the maximal dilution for which an amorphous structure is retained have several interesting properties. First, they tend to have slightly larger optical bandgaps than lower-dilution amorphous materials, which makes

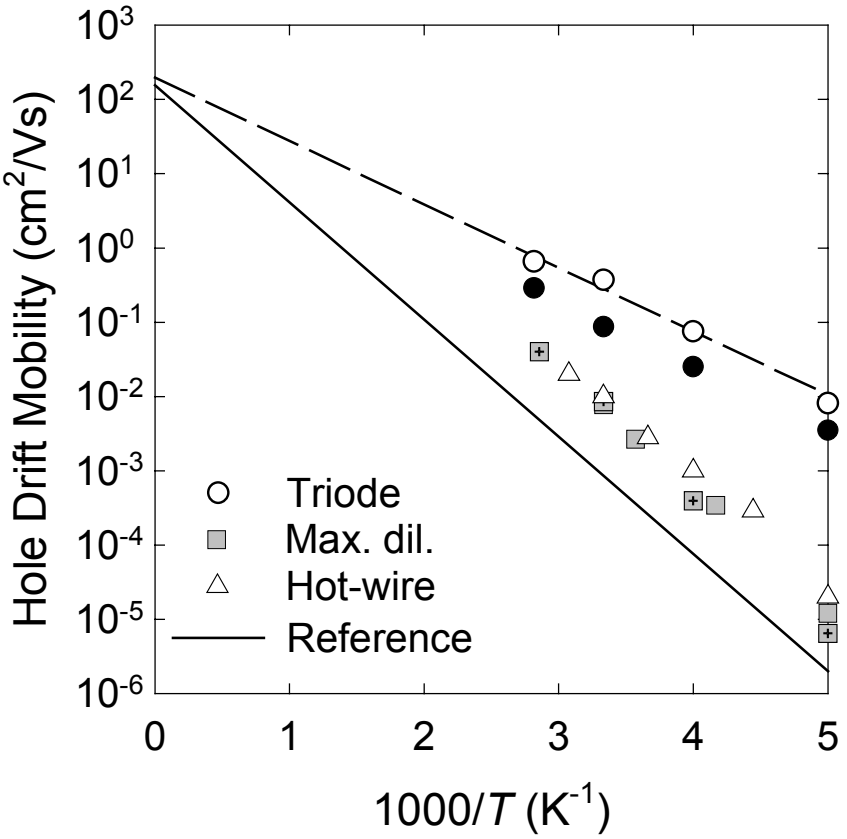

Fig. 7: Temperature-dependent hole drift mobilities for several a-Si:H samples ("triode" – deposited at Electrotechnical Laboratory, "max. dil."-maximal hydrogen dilution deposited at Penn State University, "hot-wire" deposited at National Renewable Energy Laboratory; reference deposited at United Solar Systems Corp.. Values are given for a displacement/field ratio $L/E = 2\text{x}10^{-9}$ cm^2/V;

them potentially useful for preparing high V_{OC} cells. Second, there is some evidence that maximal-dilution materials have better stabilized electronic properties than low-dilution materials. These properties must of course be considered in the context of the lower deposition rates for layers as hydrogen dilution increases.

Hole Drift Measurements

In Fig. 7 we show the temperature-dependence measured of the hole drift-mobilities for two samples of H-diluted a-Si:H along with previous measurements on triode-deposited a-Si:H, hot-wire a-Si:H [22], and a regression fit from hole measurements in conventional a-Si:H [23]. These drift-mobilities apply for a specific ratio $L/E = 2 \times 10^{-9}$ cm^2/V of hole displacement L and field E.

We have measured hole mobilities in three a-Si:H samples made at high dilution by Prof. Christopher Wronski's research group at Pennsylvania State University. The a-Si:H layers are deposited on SnO_2-coated glass (Corning 7059). The structure of the samples is glass/SnO_2/a-Si:H:P (n+)/a-Si:H (i)/Ni. The a-Si:H layers were deposited using a Tek-Vak MPS 4000-LS multi-chamber PECVD system. The intrinsic-layer deposition was done using a substrate temperature of 200 C and a hydrogen/silane ratio of 10:1. (200 C, R=H_2/SiH_4=10:1). The n+ layer was 35 nm thick and has an activation energy for electrical conduction of 0.25 eV. A top semi-transparent Schottky barrier was formed by thermal evaporation of Ni onto the intrinsic layer immediately following a short etching with buffered hydrofluoric acid; small, circular Ni electrodes of area 0.02 cm^2 were formed; the thickness of the Ni films was 15 nm. Three different samples were prepared over

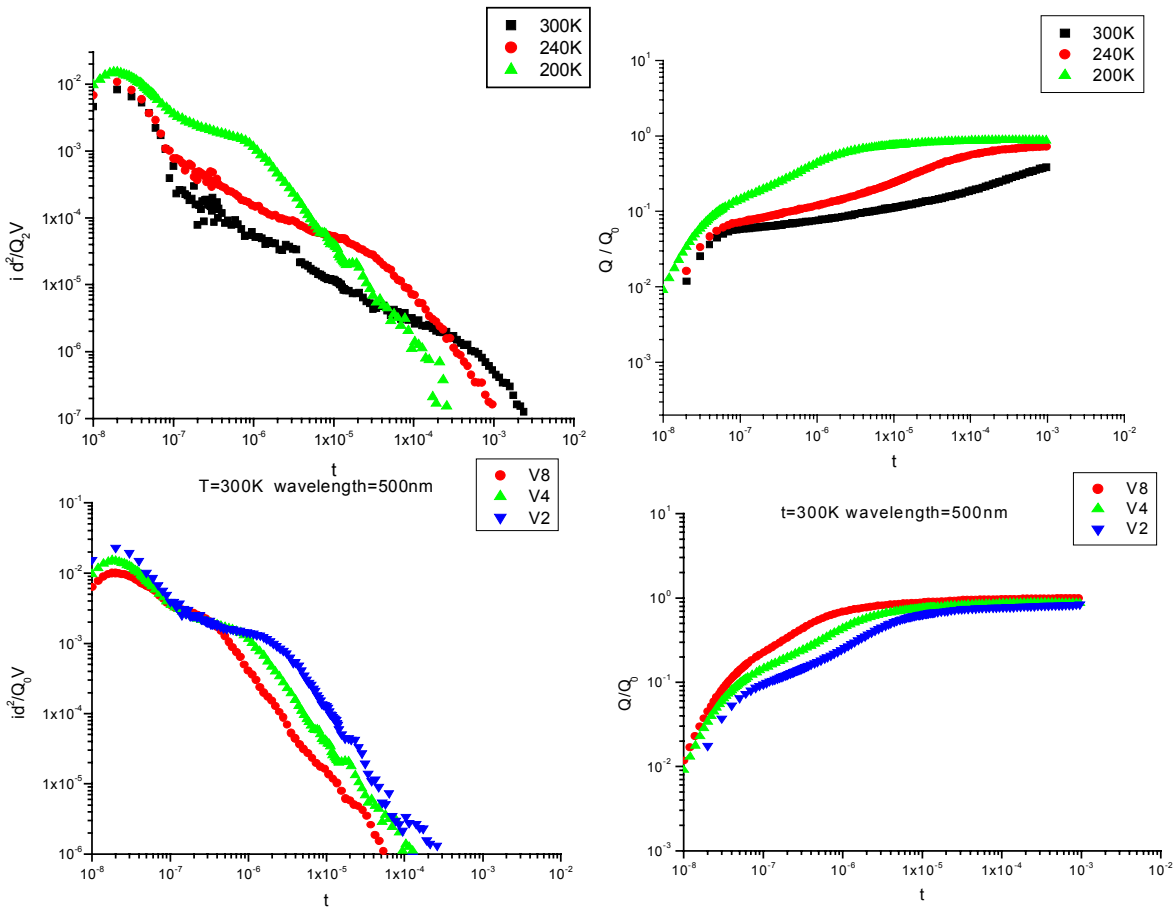

Fig. 8: Hole photocurrents measured in an a-Si:H sample made at high hydrogen dilution at Penn State University.

several months; the sample codes and their thicknesses are (CW81 - 1.1 microns, PSU 020299R – 1.5 microns, PSU 031599R - 1.47 microns). We illustrate the hole photocurrent transients measured on the third and last of these samples in Fig. 8. The transients are not remarkable, and are typical of "time-of-flight" measurements in amorphous-silicon based materials.

Fitting to the Exponential Valence Bandtail Trap Model

We have made a careful fitting study of these data using the well-known exponential bandtail trapping model [23]. As may be recalled, the three parameters of this model are the width parameter E_0 describing the exponential valence bandtail, the "attempt-to-escape" frequency ν describing hole emission from a bandtail trap, and the "microscopic mobility" μ_0 describing free drift of an untrapped hole. We summarize our fittings in the table below for the three hydrogen-diluted samples studied. We also report values from our earlier work on holes [23]. The parameters ν and μ_0 are unremarkable; they are rather difficult to establish accurately from the drift-mobility measurements, and are typically much less reproducible than the drift-mobility measurements themselves. In this context it is quite possible that the variations in the table are not significant. On the other hand, the valence bandtail width E_0 is relatively easy to establish, and indicates that the width is narrower for the hydrogen-diluted materials than for conventional amorphous silicon materials.

In previous work we found little variation of the hole drift-mobility with alloying of the amorphous silicon with germanium or with carbon, although electron drift-mobilities do vary significantly with alloying. It appears that increase in the "order" or "protocrystallinity" of amorphous silicon when it is deposited under conditions of high-hydrogen dilution have essentially the reverse effect: there is a noticeable narrowing of the valence bandtail width.

Sample	E_0 (meV)	ν (s^{-1})	μ_0 (cm^2/Vs)
Hydrogen-diluted (PSU-CW81)	40	6.3×10^{11}	0.2
Hydrogen-diluted (PSU-2)	39	1.0×10^{12}	0.3
Hydrogen-diluted (PSU 031599R)	42	2.0×10^{12}	0.6
Conventional (ECD 1689)	48	7.7×10^{10}	0.27

Table I: Exponential bandtail multiple-trapping fitting parameters.

Sub-bandgap interfacial electroabsorption in amorphous silicon

Abstract

We discuss models for the infrared spectrum peaked at 0.8 eV reported in voltage-modulation optical absorption measurements on a-Si:H based diodes. We associate this spectrum with interface charge modulation of the optical properties of the phosphorus-doped a-Si:H used as one electrode. We propose that the spectrum originates with the internal optical transitions of a complex incorporating fourfold coordinated phosphorus and a dangling bond. We discuss prior evidence against complexing, and suggest further experiments.

Introduction

We recently reported electromodulation spectra measured on diode structures incorporating intrinsic a-Si:H and a variety of *n*-type doped layers [24]. These spectra reveal the well-known electroabsorption spectrum for a-Si:H [25] which peaks near 1.8 eV (essentially the bandgap of a-Si:H). In addition we observed a variety of infrared features in the range 0.7 – 1.2 eV, and in particular a prominent peak at 0.8 eV in several samples. These latter features are most likely due to modulation of the interface charge near the *n/i* interface of the diode structures. As reverse bias is applied and removed to the diodes, charge flows onto and off of these interfaces essentially as if the sample were a simple parallel plate capacitor. We illustrate these essential results and ideas in Fig. 9. The magnitude of the optical cross-section we calculate based on the interface charge modulation model for the spectrum is 10^{-16} cm^2.

The fact that the interface-charge modulation spectrum is a fairly narrow peak surpised us; electronic

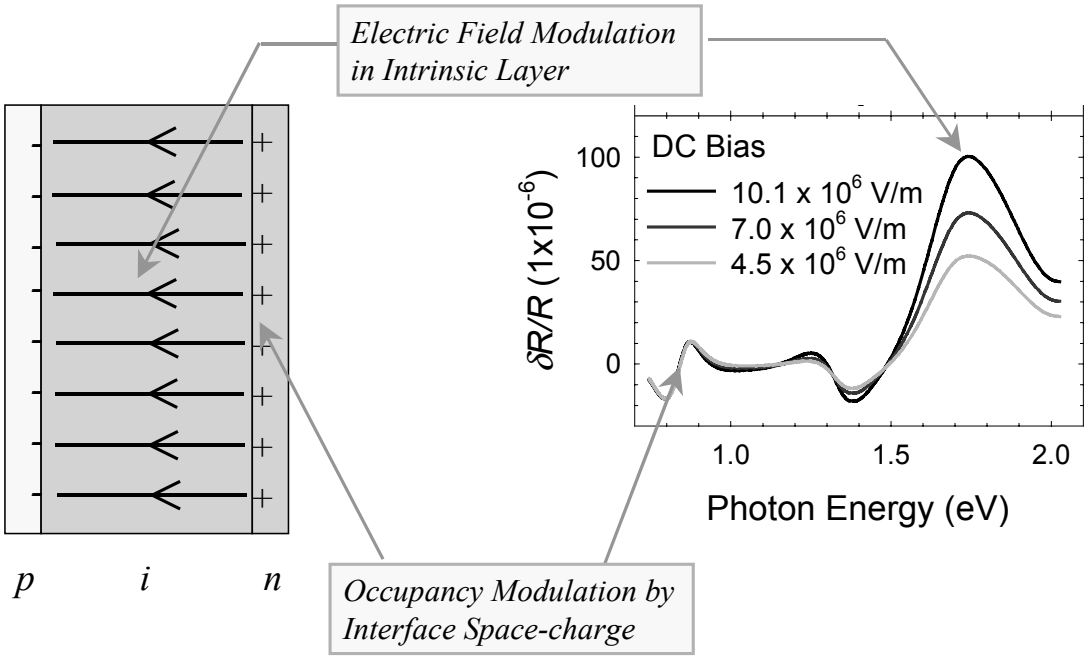

Fig. 9: The figure illustrates the interpretation of the electromodulation spectrum's two regions based on their very different scaling with reverse bias. For constant modulation amplitude, the interband electromodulation spectrum near 1.8 eV scales linearly with applied bias voltage, corresponding to true, quadratic electroabsorption in the intrinsic layer. The infrared spectrum is nearly independent of the bias, as expected from effects originating from occupancy changes near the interfaces. The sample was a pin diode for which electromodulated reflectance was measured. These spectra are affected by interference between back and front-surface reflection; ref. [24] shows spectra on additional samples without interference.

absorption spectra in a-Si:H usually consist of very broad (several eV) bands with well-defined thresholds. In the present paper we discuss two models for the spectrum. The first model is based on the standard picture for doping in n-type a-Si:H incorporating isolated, fourfold coordinated phosphorus atoms P_4 with levels near the conduction bandedge (or mobility edge). This approach doesn't appear to describe the measurements. We also discuss the spectrum for phosphorus-dangling bond complexes P_4D, which may prove a more satisfactory basis for understanding the measured spectra. In the concluding section we discuss the possible observation of P_4D in the context of the extensive prior work on doping in *n*-type a-Si:H; a convincing demonstration of a significant role for P_4D would considerably alter our views of interfaces involving *n*-type a-Si:H.

Standard Doping Model

In 1982 R. A. Street proposed a model for incorporation of phosphorus and other doping atoms into a-Si:H which appears to be a quite satisfactory basis for understanding most doping-related phenomena in a-Si:H [26]. We therefore commence by describing predictions based on this model for interface-charge modulation spectra in doped a-Si:H.

An important feature of the model for doping proposed by Street is that it accounts for the observed correlation of electrically active doping with dangling bond creation. In its simplest form, the model calls for creation of equal densities of *charged* P_4^+ and D^- (dangling bond) centers. Although there is a Coulombic energy gained if the centers are generated as intimate pairs during growth, most experiments are better explained by assuming that the centers are uncorrelated in location [26].

We therefore turn to the changes in optical properties associated with occupancy changes for bandtail states (including P_4). We use the viewpoint developed to interpret *photomodulation* spectra by J. Tauc' research group [27]; essentially the same approach was used by Eggert and Paul to interpret electromodulation spectra in a-Si:H based diodes under forward bias [28]. Electrons occuping bandtail levels (either intrinsic or doping-related) should contribute a broad band to optical absorption which starts at the threshold energy E_C-E_F for excitation of an electron to the mobility-edge. As the Fermi energy moves slightly deeper into the bandgap, and away from the bandedge, this contribution to absorption is *bleached*. We have illustrated this effect in Fig. 10. On the left we show the emptying of a bandtail level as the Fermi energy falls; to the right, the dashed line illustrates the onset of a corresponding band of bleached optical absorption (negative values for the optical cross-section σ).

Concurrent with bleaching, this motion of the Fermi energy opens up new states for a band of optical absorption involving valence-band electrons at or below the valence bandedge. The threshold for this *induced* absorption is about E_F-E_V, as illustrated by the longer arrow at the left of Fig. 2. To the right of Fig. 2 we have shown the onset of induced absorption in the continuation of the dashed curve. We have arbitrarily assumed that the induced transition has a somewhat larger optical cross-section than the bleached transition, so the net change in cross-section above the second threshold is positive [29]. At the right of Fig. 10 we also illustrate the prominent feature we measure near 0.8 eV; it is apparent that bleaching and inducing of transitions involving bandtail states is not adequate to explain the measured spectrum.

Since direct optical measurements in phosphorus doped a-Si:H indicate a threshold for the photodetachment of an electron from the D^- level of about 0.9 eV, it is plausible that this transition is somehow involved in the electromodulation spectrum. However, we do not believe that this is the correct model. We first note that depletion of isolated D^- levels in the *n*-layer is negligible, thus ruling out a direct mechanism. The application of reverse-bias to an a-Si:H based diode typically involves an interface charge of the order of 10^{-4} C/m^2, involving about 10^{11} states/cm^2. Only a very small thickness of *n*-type material is involved; at most these charges are spread through 10 nm of the material. The associated band-bending in the n-layer is thus about 0.01 V. Since the Fermi energy itself is at most 0.2 eV below the conduction bandedge in the *n*-type layer, depletion of a level 0.9 eV deep is insignificant. We have been unable to find any other mechanism for a direct influence of the Fermi energy upon the photodetachment spectrum of an isolated D^-.

Doping-Complex Model

At sufficiently high phosphorus incorporation there should be a crossover to doping involving creation of complexes of P_4 and D (denoted P_4D) [26]. We therefore examine possible optical transitions of intimate pairs as a possible origin for our interface-charge modulation spectra.

The optical spectrum associated with such a complex may be surprisingly intricate. In Fig. 11 we illustrate the proposed transitions; the transitions are further identified in Table 1. As regards the optical properties measured in response to Fermi level modulation, there is one main distinction between the properties of the complex and those of the simple bandtail level. This distinction is the presence of an internal excitation of the complex (transition 4) which is not associated with creation of a mobile electron or hole. This transition may account for the sharp, 0.8 eV spectrum we find in several diode samples. As indicated in Fig. 3, the transition is present only in the neutral complex $P_4^+D^-$, so this absorption is induced by depletion of electrons from negatively charged, $P_4^0D^-$ complexes.

We do not expect much effect in electromodulation from transitions 1 and 3; these transitions occur with comparable strength and energy for both of the charge states of the complex. We do predict absorption and bleaching bands (transitions 5 and 2, respectively) similar to those in Fig. 10. However, we have no clear evidence for such features in our observed spectra. This absence may be understood if the optical cross sections for transitions 5 and 2 are about ten times smaller than for transition 4.

We have estimated $\sigma \approx 10^{-16}$ cm^2 for transition 4 by normalizing the relative change in absorption by the number density of interface charges. This magnitude for σ is practically the same magnitude which is estimated for photodetachment of electrons from isolated D^0 and D^- centers [30,31]. We are unaware of direct measurements from which we might infer the optical cross-section for detachment of an electron from an isolated P_4^0, which we might use to infer the cross-section for transitions 5 and 2. We can only speculate as to whether the cross-section might be smaller than those involving D.

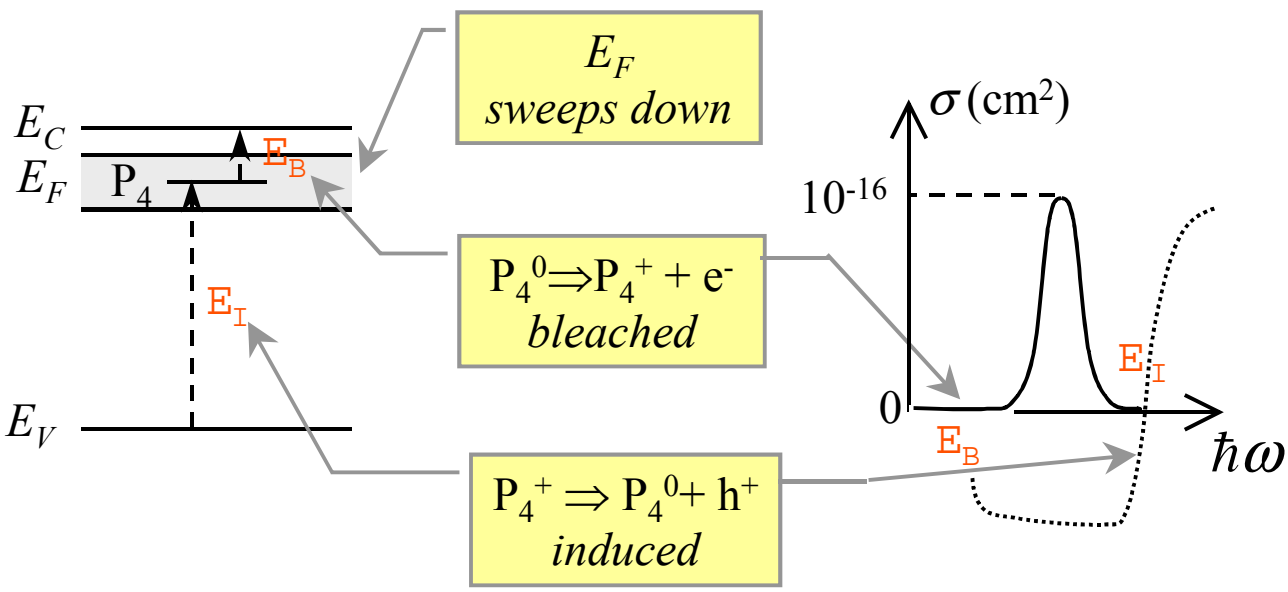

Fig. 10: Optical effects resulting from a change in the Fermi-energy in phosphorus doped a-Si:H. The drawing on the left indicates the depletion of occupied states such as P_4 near the bandedge of a-Si:H as the Fermi energy is lowered. The occupied states contribute a band to optical absorption (threshold about E_C-E_F) which is bleached when the Fermi energy falls. The bleaching band is illustrated to the right of the figure as the dashed line; bleaching accounts for the negative value for the optical cross-section σ. Depletion also opens up a final state for a band of optical transitions originating from the valence band, leading to an induced absorption above a threshold near E_F-E_V as illustrated. The solid line spectrum represents measurements on several samples.

Discussion

To date we have explored samples with four different types of *n/i* intefaces. We note that the main feature we have discussed, which is a spectral band centered at about 0.8 eV, is not present for one type of interface. There are also some weaker, highly variable spectral features which we have also not addressed here.

If we accept the proposed dominance of P_4D complexes in some types of n-type a-Si:H, we should discuss the absence of a significant density of such complexes in previous analyses [26]. The main argument is the following. "Unpaired" D and P_4 centers lead to a prediction that the densities of these centers scale as $[P]^{1/2}$ with the gas-phase phosphorus density during deposition; this prediction is reasonably consistent with published measurements on thin a-Si:H:P films. The electrical efficiency of doping thus *declines* as the phosphorus density increases. If doping were dominated by P_4D complexes, the density should scale as [P]. There is no published evidence of which we are aware supporting this latter scaling.

This argument is not (in our view) conclusive in ruling out the presence of P_4D for our particular samples. These all involve very high doping levels which are at the upper limit of the previous studies. Additionally, the present work involves interface regions which arguably may have different properties than thicker films.

The present spectroscopic argument in favor of complexes at *n/i* interfaces thus appears to us to be a plausible speculation requiring further experimental confirmation. We suggest that it would be worthwhile to repeat the earlier thin-film based studies as a function of phosphorus density using *n/i* interfaces. We would anticipate that the contribution of complexes to the interface charge modulation signal should decline with reduced doping density; the absence of the 0.8 eV band in some samples is thus further encouragement for this experiment.

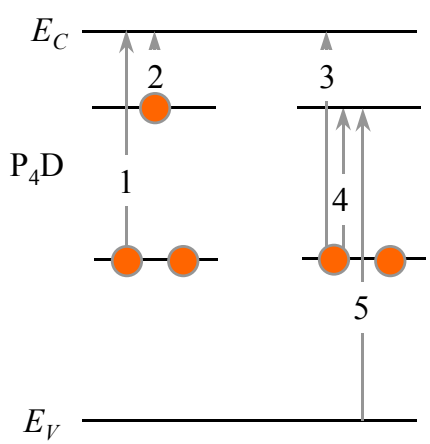

Fig. 11: A P_4D complex has five optical transitions which may contribute to optical effects. We propose that transition 4 in the diagram, which corresponds to an internal excitation of an electron from a deep level to a shallower one, is the origin of the interface-charge modulation spectrum found in infrared electromodulation measurements.

1	$P_4^0D^- \Rightarrow P_4^0D^0+e^-$	Transition from D^- to conduction band continuum
2	$P_4^0D^- \Rightarrow P_4^+D^- +e^-$	Transition from P_4^0 to conduction band continuum
3	$P_4^+D^- \Rightarrow P_4^+D^0 +e^-$	Transition from D^- to continuum
4	$P_4^+D^- \Rightarrow P_4^0D^0$	Internal transition
5	$P_4^+D^- \Rightarrow P_4^0D^-+h^+$	Transition from P_4^+ to valence band continuum

Table II: Labels and identification of five optical transitions in Fig. 11.

Hydrogen-mediated models for metastability in a-Si:H: Role of Dihydride bonding

Abstract

Two hydrogen-mediated models for defects in a-Si:H based on hydrogen pairing have previously been proposed. One model based on the clustered hydrogen phase revealed by nuclear magnetic resonance accounts well for several near-equilibrium properties, and in particular for the defect creation during hydrogen evolution. The second model based on hydrogen-collisions accounts for aspects of light-induced generation of metastable defects. We describe a unified model subsuming both models. The model is based on sites which bond two pairs of hydrogen. We discuss evidence that the site may be involved with dihydride bonding observed by infrared absorption spectroscopy.

Introduction

Practically since its discovery over 25 years ago, scientists have known that the electronic properties of hydrogenated amorphous silicon (a-Si:H) not only vary greatly from sample to sample, according to deposition conditions, but that a given sample will exhibit metastable behavior according to its history of illumination or thermal treatment. Since bonded hydrogen is clearly essential to these electronic properties, it is plausible that differing bonding arrangements may explain both types of variability. Nonetheless a comprehensive model relating hydrogen and electronic properties has never emerged.

There have been significant successes in hydrogen-mediated models for specific phenomena. In 1988 Jackson and Kakalios [32] showed that thermal annealing times for a metastable conductivity were reasonably consistent with hydrogen-diffusion measurements. In 1989, Zafar and Schiff [33] showed that the clustered phase of hydrogen revealed by nuclear magnetic resonance measurements could be used to explain how the density of dangling bonds increased as hydrogen was removed from a-Si:H in evolution experiments. Quite recently, Branz showed how the kinetics of light-induced defect generation can be explained by hydrogen collisions [34] and Biswas proposed an entirely new class of hydrogen-mediated models to account for metastabilities in optical and structural measurements [35].

In the present paper we present a proposal for marrying the hydrogen-mediated models proposed by Zafar and Schiff and by Branz. The crucial feature of both models is their assumption that hydrogen pairs can be more stable than isolated hydrogen on certain sites; the concept is reminiscent of "negative electronic correlation energies." In both models, dangling bonds are generated by transferring two hydrogen atoms bonded at isolated sites onto a single pair-site; there is thus only a single type of dangling bond which is not intimate with hydrogen. Despite the strong common feature, the models differ in a crucial detail: in equilibrium, pair-sites are mostly filled with hydrogen in the clustered-phase model, but are mostly empty in the hydrogen-collision model.

We propose here that clustered phase sites can bond two pairs of hydrogen. Under most conditions, these sites are occupied by only a single pair. When occupied by two pairs, we identify the sites with "dihydride-bonded hydrogen" often measured in a-Si:H [36]. The model predicts that annealing times for light-induced defects in "dihydride poor" a-Si:H be comparable to annealing times for thermally quenched defects in "dihydride-rich" a-Si:H; recent measurements by Quicker and Kakalios [36] appear to be consistent with this prediction.

Clustered-Phase Model

NMR measurements reveal the existence of 2 distinct environments for hydrogen in a-Si:H: "dilute-phase" hydrogen, which most likely converts to a simple dangling bond when its hydrogen is removed, and "clustered-phase" hydrogen, whose exact structure remains obscure. Zafar and Schiff [33,37] proposed the hydrogen level diagram shown in Fig. 12 (left) to account for several properties of the dangling bond density.

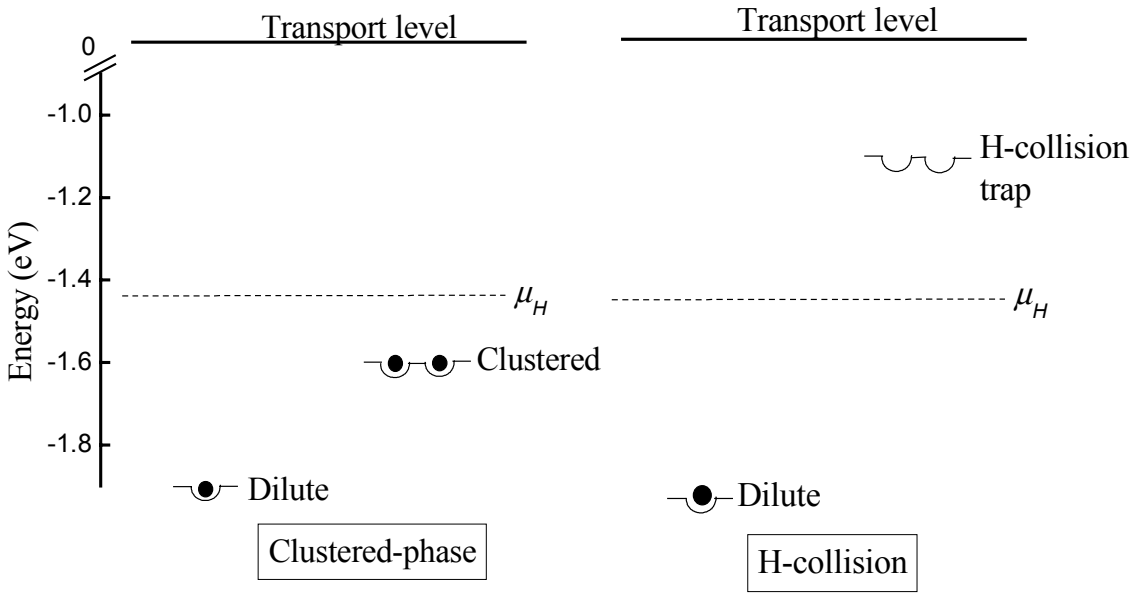

Fig. 12: Hydrogen level diagrams for the clustered-phase and hydrogen-collision models. Note that levels corresponding to both the clustered-phase and to the collision pair-trap are pair levels, implying a slight modification of ordinary one-particle statistical mechanics. The level position for the clustered phase was set to correspond to annealing measurements for thermally quenched spins; the dilute-phase level was set 0.3eV lower to account for the temperature-dependent spin density. The chemical potential is set to account for typical spin densities at 200C. For the H-collision model, the level for the pair trap was set from Staebler-Wronski annealing measurements; the dilute-phase level and the chemical potential were set the same as for the clustered-phase model. Absolute values of the level positions are set assuming that hydrogen motion is not thermally activated in the transport level

The single level associated with the clustered-phase is actually the average of level positions for the two hydrogen atoms bound at a clustered-phase site; the original paper [33] should be consulted for a more complete description of the statistical mechanics of such pair-levels. The hydrogen chemical potential μ_H is set somewhat above the clustered-phase level, so that most of the sites in both phases are occupied by hydrogen. This level diagram accounts quite accurately for measurements of the temperature-dependent dangling bond density, of the dangling bond density as hydrogen is evolved from a sample [32], and of the annealing times for metastable dangling bonds created by thermal quenching [38,39]. We have reproduced these annealing-time measurements from the literature in Fig. 13, along with annealing times from several other experiments, which we discuss subsequently.

Hydrogen-collision Model

The hydrogen-collision model developed by Branz [34] accounts for several experiments probing the transient dangling bond density during illumination. In Fig. 12 (right), we present a level diagram which we believe is consistent with the hydrogen-collision model. The main change *vis a vis* the clustered-phase model is a raising of the pair-level above the chemical potential μ_H. The raising permits the H-collision model to account for two important aspects of light-induced dangling bonds. First, the activation energy for annealing of light-induced dangling bonds is significantly smaller than the activation energy for annealing of metastable dangling bonds created by thermal quenching. The experimental data on annealing times for quenched [38,39] and for light-induced [40,1,41] defects is presented in Fig. 13. The pair levels positions below the H-transport level in Fig. 12 were set to correspond with the activation energies in Fig. 13 (1.6 eV for quenched dangling bonds, 1.1 eV for light-induced) [42].

The second aspect requiring a pair level above μ_H is light-induced annealing, which is invoked to account for the steady-state dangling bond density reached after long illumination. In the hydrogen-collison model, light-induced detrapping of H-pairs is negligible in equilibrium, but rises proportional to the density of hydrogen trapped in pair-sites. Ultimately a balance is reached by light-induced H-generation from dilute phase sites, and light-induced detrapping from pairs. These properties require that the initial density of H on the pair-level be much less than the density of empty-sites for the dilute level (ie. much less than the initial dangling bond density). Correspondingly, the chemical potential must satisfy:

$$(\mu_H - E_D) < 2(E_P - \mu_H) \tag{1}$$

where E_D and E_P denote the dilute and pair level positions, respectively. μ_H is evaluated at about 200 C, since room-temperature spin densities are quenched in around 200 C. We have assumed that the densities of dilute-phase and pair-trap levels are equal. The factor 2 emerges from the properties of pair levels. It is noteworthy that the level positions in Fig. 12, which were chosen to match several activation-energy experiments, satisfy this constraint without adjustment.

The Dihydride Model

It is essential to marry these two models to have any claim to a comprehensive view of dangling bonds and hydrogen in a-Si:H. We propose the level diagram presented in Fig. 14. The key assumption is that clustered-phase sites can now bind either one or two hydrogen-pairs. The marriage is fairly uncomplicated: the thermal equilibrium properties are largely controlled by the lower pair level, whereas non-equilibrium properties such as the Staebler-Wronski effect can be dominated by the upper level.

Since this newly proposed model mainly joins less comprehensive models for defects and hydrogen, it largely inherits their desirable properties without predicting much which is new. However, we furthermore propose that dihydride bonding, which is frequently observed in a-Si:H, corresponds to the upper pair level of a clustered-phase site. We have illustrated the identification of levels with bonding configurations in Fig. 14.

This dihydride-bonding proposal admits at least one new experimental test. In Fig. 13, we compare annealing times for dangling bonds in dihydride-rich material with annealing times for light-induced spins in conventional a-Si:H, which has little dihydride-bonding. Although there is precious little published data on equilibration times in dihydride rich material, the one datum does appear similar to the annealing times for light-induced defects in normal a-Si:H. While certainly not a conclusive test, this coincidence, which has not to our knowledge been noticed before, indicates that a more thorough examination of the "dihydride" model may be fruitful.

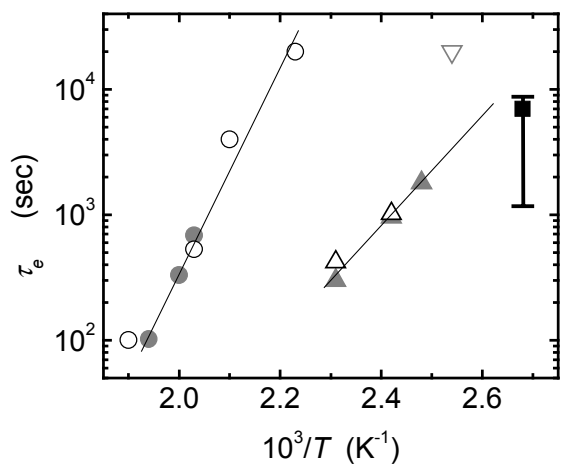

Fig. 13: Annealing times for quenched defects (circles) and for light-induced defects (triangles). The data points were taken from the literature: solid circles [38], open circles [39], solid triangles [32], open up-triangles [40], open down-triangle [41]. Annealing time for dihydride-rich material is shown as a square with a corresponding error bar. This data point was taken from ref [36]. The lines present thermally activated process with activation energy 1.6 eV for quenched and 1.1 eV for light-induced defects.

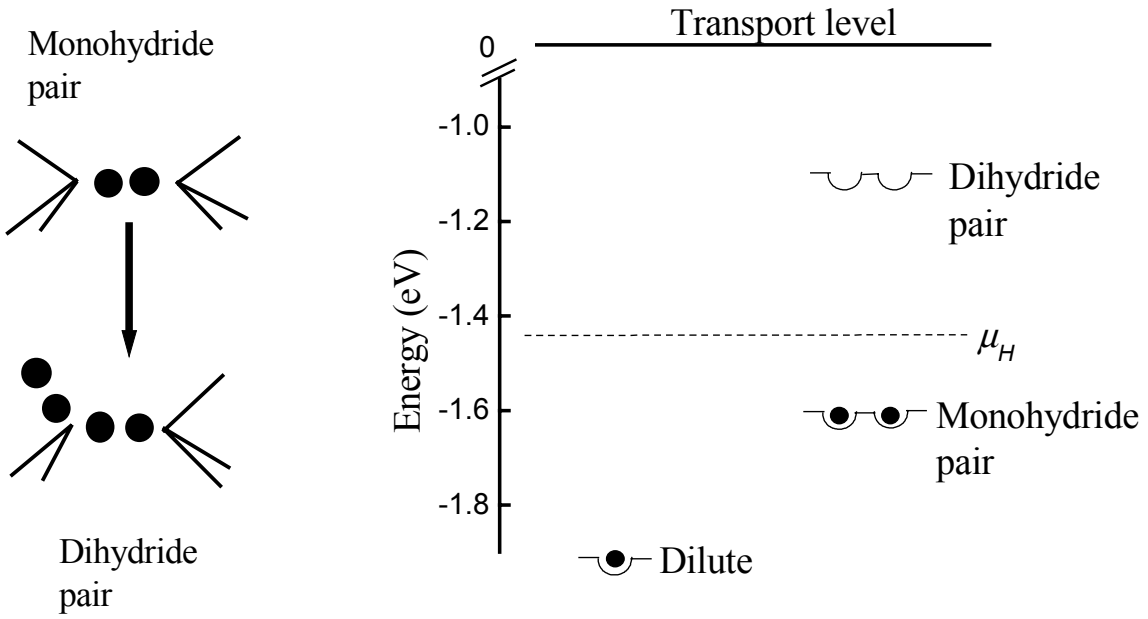

Fig. 14: Hydrogen level diagram and bonding configurations for the dihydride model. Note that monohydride and dihydride states are pair levels.

References

1. H. Zhu and S. J. Fonash, collected in *Amorphous and Microcrystalline Silicon Technology - 1998*, edited by R. Schropp, *et al.* (Materials Research Society, Symposium Proceedings Volume 507, Pittsburgh, 1998), 395.

2. A. Rose, *Photoconductivity and Allied Topics* (Wiley, 1963, New York; reprinted Krieger, 1978).

3. S. J. Fonash, *Solar Cell Device Physics* (Academic, New York, 1981).

4. Despite the fact that this result is well known, we are unaware of any conclusive proof, which would indicate its limitations.

5. S. Wagner, X. Xu, X. R. Li, D. S. Shen, M. Isomura, M. Bennett, A. E. Delahoy, X. Li, J. K. Arch, J.-L. Nicque, and S. J. Fonash, in *Conference Record of the IEEE Photovoltaic Specialists Conference* (Institute of Electrical and Electronics Engineers, New York, 1991), 1307.

6. F. Wang and R. Schwarz, *J. Appl. Phys.* **71**, 791 (1992).

7. T. Tiedje, *Appl. Phys. Lett.* **40**, 627 (1982). A calculator based on Tiedje's expressions is currently available at the web-site http://physics.syr.edu/~schiff/AMPS.

8. L. Jiang, E. A. Schiff, Q. Wang, S. Guha, and J. Yang, *Appl. Phys. Lett.***69**, 3063 (1996).

9. S. Guha, J. Yang, P. Nath, and M. Hack, *Appl. Phys. Lett.* **49**, 218 (1986).

10. Q. Wang, E. Iwaniczko, Y. Xu, W. Gao, B. Nelson, H. Mahan, R. S. Crandall, H. M. Branz, *this volume*.

11. H. M. Branz and R. S. Crandall, *Solar Cells* **27**, 159 (1989).

12. I.-S. Chen and C. R. Wronski, J. Non-Cryst. Solids 190, 58 (1995).

13. W. B. Jackson, S. M. Kelso, C. C. Tsai, J. W. Allen, and S.-J. Oh, *Phys. Rev. B* **31**, 5187 (1985).

14. E. A. Schiff, R. I. Devlen, H. T. Grahn, J. Tauc, and S. Guha, *Appl. Phys. Lett.* **54**, 1911 (1989).

15. G. Juska, K. Arlauskas, J. Kocka, M. Hoheisel, and P. Chabloz, *Phys. Rev. Lett.* **75**, 2984 (1995).

16. Q. Wang, H. Antoniadis, E. A. Schiff, and S. Guha, *Phys. Rev. B* **47**, 9435(1993).

17. E. A. Schiff, *J. Non-Cryst. Solids* **190**, 1 (1995).

18. Q. Gu, Q. Wang, E. A. Schiff, Y.-M. Y.-M., and C. T. Malone,*J. Appl. Phys.* **76**, 2314 (1994).

19. G. Juska, J. Kocka, M. Viliunas, and K. Arlauskas, *J. Non-Cryst. Solids* **164-166**, 579 (1993).

20. P. Stradins, H. Fritzsche, P. Tzanetakis, and N. Kopidakis, in *Amorphous Silicon Technology - 1996*, edited by M. Hack, *et al* (Materials Research Society Symposium Proceedings Vol. 420, Pittsburgh, 1996), p. 729.

21 S. Guha, J. Yang, D. L. Williamson, Y. Lubianiker, J. D. Cohen, and A. H. Mahan, *Appl. Phys. Lett.* **74**, 1860 (1999).

22 E. A. Schiff, Q. gu, L. Jiang, J. Lyou, I. Nurdjaja, and P. Rao, *Research on High-Bandgap Materials and Amorphous Silicon-Based Solar Cells: Final Technical Report* (NREL document SR-520-25922, 1998), p. 31.

23 Q. Gu, Q. Wang, E. A. Schiff, Y.-M. Li, and C. T. Malone, *J. Appl. Phys.* **76**, 2310 (1994).

24 J. Lyou, E. A. Schiff, S. S. Hegedus, S. Guha, and J. Yang, in *Amorphous and Heterogeneous Silicon Thin Films: Fundamentals to Devices (1999)*, edited by H. M. Branz, R.W. Collins, H. Okamoto, S. Guha, R. Schropp (Materials Research Society, Symposium Proceedings Vol. 557, Pittsburgh), *in press.*

25 G. Weiser, U. Dersch, and P. Thomas, *Phil. Mag. B* **57**, 721 (1988).

26 R. A. Street, *Hydrogenated Amorphous Silicon* (Cambridge University Press, Cambridge, 1991).

27 Z. Vardeny and J. Tauc, *Phys. Rev. Lett.* **54**, 1844 (1985).

28 J. R. Eggert and .W. Paul, *Phys. Rev. B* **35**, 7993 (1987).

29 W. B. Jackson, S. M. Kelso, C. C. Tsai, J. W. Allen, and S.-J. Oh, *Phys. Rev. B* **31**, 5187 (1985) discuss the "random phase" conjecture that the matrix elements for all of these optical transitions are the same.

30 A. V. Gelatos, J. D. Cohen, and J. P. Harbison, J. Non-Cryst. Solids **77&78**, 291 (1985).

31 W. B. Jackson and N. M. Amer, *Phys. Rev. B* **25**, 5559 (1982).

32. W.B. Jackson and J.Kakalios, *Phys. Rev. B* 37 (1988) 1020.

33. S. Zafar and E. A. Schiff, *Phys. Rev. B* 40 (1989) 5235.

34. H. Branz, *Sol. State Commun.* 105/6 (1998) 387, H. Branz, *Phys. Rev. B* 59 (1999) 5498.

35 R. Biswas and Y.-P. Li, *Phys. Rev. Lett,* 82 (1999) 2512

36. Quicker and J. Kakalios, *Phys. Rev. B*. 60 (1999) 2449.

37. S. Zafar and E. A. Schiff, *Phys. Rev. Lett,*.66 (1991) 1493

38. S. Zafar and E. A. Schiff, *J. Non-Cryst. Solids* 137&138 (1991)

39. X. Xu, H. Sasaki, A. Morimoto, M. Kumeda, T. Shimitzu, *Phys. Rev. B* 41 (1990) 10049.

40. M. Stutzmann, W. B. Jackson, and C.-C. Tsai, *Phys. Rev. B* 32 (1985) 23.

41. Q. Zhang, H. Takashima, J-H. Zhou, M. Kumeda, T. Shimitzu, *Mat. Res. Soc. Symp. Proc.* 336 (1994) 269.

42. An interesting property of pair levels is that their positions, and not that of μ_H, determine measured activation energies.

REPORT DOCUMENTATION PAGE

Form Approved
OMB NO. 0704-0188

1. AGENCY USE ONLY (Leave blank)	2. REPORT DATE February 2001	3. REPORT TYPE AND DATES COVERED Subcontract Report, 24 March 1999 – 23 March 2000

4. TITLE AND SUBTITLE Electroabsorption and Transport Measurements and Modeling Research in Amorphous Silicon Based Solar Cells 6. AUTHOR(S) E. A. Schiff, N. Kopidakis, J. Lyou, S. Rane, Q. Yuan, and K. Zhu	5. FUNDING NUMBERS C:XAK-8-17619-23 TA: PVP1.5001
7. PERFORMING ORGANIZATION NAME(S) AND ADDRESS(ES) Syracuse University Syracuse, New York	8. PERFORMING ORGANIZATION REPORT NUMBER
9. SPONSORING/MONITORING AGENCY NAME(S) AND ADDRESS(ES) National Renewable Energy Laboratory 1617 Cole Blvd. Golden, CO 80401-3393	10. SPONSORING/MONITORING AGENCY REPORT NUMBER NREL/SR-520-29504

11. SUPPLEMENTARY NOTES

NREL Technical Monitor: Bolko von Roedern

12a. DISTRIBUTION/AVAILABILITY STATEMENT National Technical Information Service U.S. Department of Commerce 5285 Port Royal Road Springfield, VA 22161	12b. DISTRIBUTION CODE

13. ABSTRACT *(Maximum 200 words)*

We have performed computer calculations to explore effects of the *p/i* interface on the open-circuit voltage in a-Si:H based *pin* solar cells. The principal conclusions are that interface limitation can occur for values of V_{OC} significantly below the built-in potential of V_{BI} of a cell, and that the effects can be understood in terms of thermionic emission of electrons from the intrinsic layer into the *p*-layer. We compare measurements of V_{OC} and electroabsorption estimates of V_{BI} with the model calculations. We conclude that *p/i* interface limitation is important for current a-Si:H based cells, and that the conduction band offset between the *p* and *i* layers is as important as the built-in potential for future improvements to V_{OC}

14. SUBJECT TERMS pin solar cells; electroabsorption; p/I; transport measurements; modeling research; amorphous silicon; open-circuit voltage	15. NUMBER OF PAGES 16. PRICE CODE

17. SECURITY CLASSIFICATION OF REPORT	18. SECURITY CLASSIFICATION OF THIS PAGE	19. SECURITY CLASSIFICATION OF ABSTRACT	20. LIMITATION OF ABSTRACT
Unclassified	Unclassified	Unclassified	UL